Inelastic energy loss in 100-keV H^+ scattering from single atoms: Theory and experiment for K, Rb, and Cs

A. Hentz,[1,2] G. S. Parkinson,[1] A. J. Window,[1] P. D. Quinn,[1] D. P. Woodruff,[1,*] P. L. Grande,[2] G. Schiwietz,[3] P. Bailey,[4] and T. C. Q. Noakes[4]

[1]*Physics Department, University of Warwick, Coventry CV4 7AL, United Kingdom*

[2]*Universidade Federal do Rio Grande do Sul, Instituto de Fisica, Avenida Bento Gonçalves 9500, 91501-970 Porto Alegre, RS, Brazil*

[3]*Hahn-Meitner-Institut, Abteilung SF4, Bereich Strukturforschung, Glienicker Strasse 100, 14109 Berlin, Germany*

[4]*CLRC Daresbury Laboratory, Daresbury, Warrington WA4 4AD, United Kingdom*

(Received 19 April 2006; published 6 September 2006)

The energy-loss spectrum associated with scattering of 100-keV H^+ ions from K, Rb, and Cs atoms adsorbed on Al(111) has been investigated both experimentally and theoretically. Theoretical simulations were conducted based on calculations of the energy loss experienced in specific ion trajectories at the surface, using coupled-channel calculations to describe inner-shell ionization and excitation as a function of impact parameter. The energy losses can be attributed entirely to single atomic collisions from the alkali atoms, and the experiments reproduce the markedly increased asymmetry in scattering from Rb and Cs relative to K, attributable largely to the role of 3*d* and 4*d* excitations, respectively, and particularly the role of multiple excitations of these states. For Rb and Cs scattering, the data show excellent quantitative agreement between theory and experiment; for the K scattering, a discrepancy of a low-energy shoulder is attributed to a problem associated with the sample preparation.

DOI: 10.1103/PhysRevB.74.125408 PACS number(s): 68.49.Sf, 79.20.Rf, 34.50.Bw, 34.50.Dy

I. INTRODUCTION

Medium energy ion scattering (MEIS),[1] typically using 100-keV incident H^+ or He^+ ions, is increasingly applied to a range of problems concerned with compositional and structural characterization of the near-surface region of solids. The technique is closely related to conventional (MeV) Rutherford backscattering (RBS), but the higher spectral resolution possible through the use of dispersive electrostatic energy analyzers at the lower ion energies provides the possibility of substantially superior (atomic-scale) depth resolution. In both techniques the energy of the scattered ions is determined by the recoil energy loss, which depends on the mass of the scattering atom, and by the inelastic loss, which varies with the distance traveled by the ions through the solid. This distance of travel depends on the depth of the scatterer, so the scattered ion energy spectrum contains information on both the depth and elemental character of atoms in the near-surface region.

If the ions travel through many atomic layers in the solid, it is usually sufficient to relate the total inelastic energy loss to the depth of the scatterer through an average energy loss per unit distance traveled in the sample, typically calculated using the SRIM code,[2] which takes no account of the crystallographic character of the sample. In reality, of course, the energy loss is due to discrete electronic excitations, which are thus stochastic in nature. One consequence of this is a broadening of the scattered ion energy peak by an amount which increases with increasing depth due to variations in the number of discrete losses. Empirical formulae can be applied to estimate this "straggling" effect (e.g., Refs. 3 and 4). These approximate methods work well in RBS, but if one wishes to exploit fully the atomic-scale depth resolution in MEIS it is important to describe more explicitly the details of the specific electronic energy-loss processes that occur and their relative probabilities.

Evidently, to extract the full depth information from MEIS spectra from the outermost few atomic layers of a solid, one requires a more sophisticated approach which must contain two key ingredients, namely (i) a detailed description of the energy losses involved in scattering from a single atom and (ii) explicit inclusion of each of these single-atom collision effects along the scattering trajectory of an ion passing through the surface region. Computer codes to implement this approach have recently been introduced by some of us, as described below. Specifically, the energy losses in single-atom collisions as a function of impact parameter are described in a formulation based on *ab initio* quantum mechanical methods using full numerical atomic-orbital coupled-channel calculations.[5] The combined energy losses through interactions with all nearby surface atoms close to the ion trajectory are then included through the use of a computer program SILISH (SImulation of LIne SHape), which incorporates the results of the single-atom collision losses into a Monte Carlo calculation of the ion trajectories through the solid. This complete approach has already been applied to MEIS from the clean Al(110) surface and compared with experimental data with generally encouraging results,[6] although there do appear to be some detailed discrepancies between theory and experiment. A recent application to MEIS data from Cu(111) displays similar effects.[7]

While these measurements of scattering from clean elemental surfaces provide relatively simple tests for the theoretical modeling, they do involve scattering trajectories which involve interaction with several near-surface atoms at different impact parameters, even in so-called "double-alignment" geometries in which the incident and detected ion directions are chosen to maximize the importance of shadowing due to elastic scattering in order to restrict the number of contributing atomic layers. Of course, a proper description of these multiple energy losses is the ultimate objective, but

to test the methods in detail it is helpful to first establish the accuracy of the single-atom energy-loss component of the theory. For this purpose special experiments are required in which submonolayer coverages of the atoms of interest are deposited onto a substrate of lower atomic mass (to ensure that ions scattered from the substrate emerge at lower energies and so do not influence the scattered ion energy spectrum from the adatoms). Further requirements are that the deposited atoms do not form three-dimensional clusters, and do occupy adsorption sites above the surface, both necessary if the ions scattered from the adatoms are to undergo significant energy losses only in the single hard collision from a single adatom.

Our first attempt to conduct such a test involved MEIS measurements from monolayer and submonolayer coverages of Y atoms on Si(111).[8] Y is more massive than the Si substrate and has the added advantage that it occurs only with a single isotopic mass, thus avoiding broadening of the scattered ion energy spectra due to different elastic recoil energy loss. This system is also known to form a structurally characterized monolayer (1×1) surface silicide.[9] However, this silicide phase does have the Y atoms in subsurface sites, and SILISH calculations showed that this geometry led to energy loss to nearby Si atoms in the incident and scattered ion trajectories. There was also evidence of adatom clustering, so although the results showed that for near-normal incidence and detection there was reasonable agreement between theory and experiment, the data failed to provide the simple single-atom scattering data required.

Here we present the results of a combined theory/experiment study of 100-keV H^+ scattering from the alkali metal atoms K, Rb, and Cs deposited on Al(111), a group of adsorption systems that appear to satisfy our requirements more fully. These adsorption systems have been characterized rather fully in many previous studies.[10] Typically, alkali adatoms are in an ionic state, giving up most or all of their one outer-shell valence electron to the substrate; this leads to the large surface dipole moment responsible for a pronounced lowering of the work function, and ensures that clustering does not occur. Moreover, at room temperature, none of these species can be deposited to overlayer coverages in excess of a single atomic layer. Rather complete quantitative structural information is available for K and Rb on Al(111).[11–14] At low temperature, these species surprisingly form $(\sqrt{3}\times\sqrt{3})R30°$ surface phases in which the adatom occupies sites atop the surface layer Al atoms, but at room temperature the alkali atoms displace some of the surface layer Al atoms to form substitutional surface alloys (that retain the $(\sqrt{3}\times\sqrt{3})R30°$ periodicity). An important feature of these surface alloy phases, however, is that because of the large effective radii of the alkali metal atoms, the outermost alloy layer is very heavily rumpled, with the alkali atoms much higher above the surface than the surrounding Al atoms. SILISH calculations reveal no discernible difference in the predicted scattered ion energy spectrum from the atop overlayer and surface alloy phases, except at very grazing ion trajectories, confirming than even in these alloy phases true single-scattering can be expected from the protruding alkali atoms. For Cs on Al(111), a low-temperature $(\sqrt{3}\times\sqrt{3})R30°$ phase involves atop adsorption,[15] as for K and Rb, but at room temperature a $(2\sqrt{3}\times2\sqrt{3})R30°$ phase occurs for which there is no complete structure determination but evidence of the same surface alloying seen for the other alkalis,[15,16] which we can rather reliably assume places the Cs atom centers above those of the Al surface atoms, particularly as Cs has the largest atomic radius of any of these adatoms.

Apart from these attractive structural aspects, the three alkali atoms have other aspects which make them of interest for this study. Not only are all three atoms more massive than Al that comprises the substrate, but Cs has essentially only a single naturally occurring isotope; Rb and K are both dominated by two isotopic masses at 85 amu (22%) and 87 amu (78%) for Rb, and at 39 amu (93%) and 41 amu (7%) for K, so in these cases some broadening of the scattered ion energy spectra arises from this source. The relative binding energies and occupancies of shallow core levels, the excitation of which leads to the inelastic loss asymmetry in the scattered ion energy spectrum, also show interesting differences. These are:

K: 370 eV $(2s^2)$; 301 eV $(2p^6)$; 41 eV $(3s^2)$; 25 eV $(3p^6)$,

Rb: 303 eV $(3s^2)$; 239 eV $(3p^6)$; 122 eV $(3d^{10})$; 37 eV $(4s^2)$; 21 eV $(4p^6)$,

Cs: 216 eV $(4s^2)$; 170 eV $(4p^6)$; 89 eV $(4d^{10})$; 30 eV $(5s^2)$; 18 eV $(5p^6)$,

where the binding energies given are the Hartree-Fock-Slater values used in the theoretical calculations presented here; these typically differ by a few eV from experimental tabulated photoelectron binding energies.[17] A conspicuous difference between K on the one hand and Rb and Cs on the other hand is the probable influence of the *d* electron states. For K, with no occupied *d*-states, the dominant shallow core level excitations are likely to be those of the 3*s* and 3*p* electrons with binding energies that are small compared with the typical instrumental resolution of 200–300 eV, so the resulting asymmetry in the experimental scattered ion energy spectrum due to inelastic losses is likely to be weak, as the cross section for excitation of the deeper 2*s* and 2*p* states will be low. In Rb and Cs one has similar shallow (4*s*, 4*p* and 5*s*, 5*p* respectively) core levels with small binding energies and high cross sections, and deeper states (3*s*, 3*p* and 4*s*, 4*p*, respectively) with small cross sections, but in addition these atoms have the high-occupancy *d* states with intermediate binding energies which may be expected to lead to significantly larger asymmetry in the experimental scattered ion energy spectra.

II. EXPERIMENTAL DETAILS

The experiments were performed at the Daresbury Laboratory UK National MEIS facility.[18] The ion accelerator is fitted with a duoplasmatron ion source and was operated for the present studies with a H^+ beam at a nominal energy of

100 keV. The end station consists of separate ultrahigh vacuum (UHV) chambers for sample preparation and characterization, for sample storage, and for the ion scattering experiments. Samples are introduced into the preparation chamber via a fast-entry load-lock and transferred between chambers under UHV conditions. MEIS measurements were performed with the sample at room temperature. The sample was aligned with respect to the incoming ion beam by means of a high-precision goniometer. The position of the beam spot on the sample surface was changed regularly to minimize ion-induced damage. The maximum ion dose used on any one spot on the sample was 10 μC of ion charge, corresponding to approximately 2×10^{16} ions/cm^2 for the high-resolution measurements reported here. Ions scattered from the sample were detected by a moveable toroidal electrostatic analyzer, the two-dimensional (2D) detector[19] of which provides "tiles" of ion counts as a function of both ion energy and scattering angle over limited ranges of each.

The general methodology for extracting ion energy spectra and angular blocking curves from these raw data tiles has been described elsewhere.[18,20] In the present experiments, however, for which our objective is to collect scattered ion energy spectra of good signal-to-noise quality at high spectral resolution, a modified method, described previously in the context of our study of Y on Si(111),[8] was adopted. In particular, in order to optimize the resolution, the three sets of slits in the beamline that define the beam size and divergence were closed down, decreasing the vertical size of the ion beam (perpendicular to the scattering plane but within the dispersion plane of the analyzer) from 0.5 mm to 0.15 mm. This led to a reduction of the effective ion beam current, from ~60 nA to ~20 nA, but an improvement in the overall energy resolution (full width at half maximum—FWHM) in the measured spectra from ~400 eV to ~250 eV. Of course, the reduced beam current leads to a loss of signal, and thus a deterioration in the statistical noise, for the same data collection times. To address this problem, scattered ion energy spectra taken at slightly different scattering angles (within the 2D detector angular range) were displaced in energy by the kinematic factor (the change in recoil energy loss with scattering angle) and then summed over a finite angular range. To allow for any nonlinearities in the 2D detector,[21,22] the kinematical correction factor was extracted from the data by fitting to the scattered ion energy peak in each angular channel of the detector, as described previously.[8] This procedure worked well for the Rb and Cs scattering data, but proved a problem for the K scattering data, because the scattering cross section is so much lower that the signal-to-noise ratio in an individual channel was too poor to provide reliable fitting. For the K scattering data, therefore, no correction could be made for a known "sawtooth" distortion in the two-dimensional detector; as a result, the K scattering data is expected to show slight additional energy broadening due to this effect.

A single channel in the detector corresponds to an angular range of 0.15°, and in the data presented here the spectra are averaged in this way over ten such channels. Notice that in all figures showing the experimental data, the energy scale is offset by the kinematic correction factor (referred to hereafter as "*k*-offset"), and so does not include the recoil energy loss of the main scattering collision. As we are concerned here only with the relative energies within the spectra that define the energy losses, this offset of the absolute energy scale is of no consequence. Indeed, small variations in the primary beam energy from experiment to experiment associated with the operating conditions of the ion source also occurred, and additional small energy shifts (typically up to ~200 eV) in the absolute energy scale have been applied to different spectra to simplify comparisons between them. The same nominal absolute energies are also used for the matching theoretical simulations.

The Al(111) crystal, initially spark-machined from an oriented single-crystal bar and mechanically polished, was cleaned *in situ* by the usual combination of ion bombardment and annealing until a clean well-ordered surface was obtained as judged by Auger electron spectroscopy and low-energy electron diffraction (LEED). Initially 1 keV Ar^+ ion sputtering was used, but small amounts of embedded subsurface Ar, even after quite extensive annealing at 400 °C, proved difficult to remove and led to a scattering signal in MEIS only slightly lower in energy than that from K deposited on the surface. For this reason, Ne^+ sputtering was used for all the data reported here although, as remarked below, some subsurface implanted Ar may have remained in the sample from the earlier cleaning treatment. The alkali metals were deposited from well-outgassed SAES "Getter" sources heated by passing currents of typically 6.5–7.5 A through them. For K and Rb the nominal saturation dose at room temperature yielded $(\sqrt{3}\times\sqrt{3})R30°$ LEED patterns, while for Cs a rather weak set of extra LEED beams attributable to the $(2\sqrt{3}\times2\sqrt{3})R30°$ phase was seen.

III. THEORETICAL DETAILS

As mentioned in the introduction, the theoretical treatment required to compare with these experimental results requires two stages. In the first stage the details of the inelastic energy losses associated with interaction with a single scattering ion are described. These results are then incorporated into a simulation of the ion trajectories through the surface region in the experiment. This procedure has been described more fully previously,[8] but we summarize the main points below.

A. Inelastic excitations in single collisions

In order to determine the inelastic energy-loss distribution in a single atomic collision, we have applied methods well established in atomic physics, namely the solution of the time-dependent Schrödinger equation for one active electron (through so-called close-coupled calculations) in the independent-electron model (IEM).

Coupled-channel calculations are the best tool to describe inner-shell ionization and excitation of atoms[23] as a function of the impact parameter. These time-consuming calculations are based on the semiclassical method.[24] The projectile (incident ion) following a classical trajectory provides a time-dependent electrostatic perturbation on the target electrons which is incorporated in a full solution of the time-dependent

Schrödinger equation. For a given impact parameter b, the amplitudes $a_{i\to f}$ are calculated for any transition from an initial occupied state i to an unoccupied bound or continuum state f of the target atom and thus the probability corresponding to atomic excitation or ionization is determined. From such calculations we obtain the energy loss or energy transfer (T) probability, dP/dT, for each atomic subshell as a function of the impact parameter, b. This contains a nonzero probability for no-loss collisions, $dP_{\text{no-loss}}/dT$, realized by a delta function, and the function dP_{loss}/dT for $T>0$ that is continuous apart from some spikes due to excitations to bound states. Details of the atomic orbital coupled-channel calculations (AO) may be found elsewhere. Notice that the calculations used here take no explicit account of electron capture by the H^+ ion but this is known to be a weak effect ($\sim 5-10\%$) for 100 keV H^+. Furthermore, as shown previously, the use of the huge basis set of final states does take account of energy loss due to electron capture reasonably well. We also note that the inner-shell ionization/excitation probabilities at these energies are very similar for H^+ and H^0 due to the large screening radius of H^0 relative to the inner-shell radii. Of course, the experiments to which we compare our theoretical results involve detection only of H^+ ions, so any H^0 species leaving the surface do not contribute to the measured signal.

The calculations have been performed for each active electron in a given subshell in the framework of the frozen-core Hartree-Fock-Slater method.[25] Fano-Lichten[26,27] type promotion typically does not occur for such asymmetric projectile-target systems. Furthermore, adiabatic changes of the target-electron densities are small for $Z_1 \ll Z_2$. Thus, the frozen-core Hartree-Fock method should be quite reliable. All probabilities, dP/dT, were then combined according to the independent-electron model to allow for energy losses involving more than one electron (multiple excitation and ionization events). Thus, for example, considering a hypothetical atom with only two electrons, the probability for a certain total electronic energy loss, ΔE, transferred during an individual ion-atom collision, can be written as

$$\frac{dP_{atom}^{elec}}{d\Delta E} = \int \left[g_1 \delta(T_1) + \frac{dP_{loss}}{dT_1} \right] \left[g_2 \delta(T_2) + \frac{dP_{loss}}{dT_2} \right] \times \delta[\Delta E - (T_1 + T_2)] dT_1 dT_2, \quad (1)$$

where the probability for a no-loss collision, g_i, for each electron, i, appears explicitly. The terms in the product of probabilities within the integral describe the probability of the two electrons being found in their original state after the ion-atom collision, the probability for single excitation or ionization events (one term for each electron), and finally the probability that both electrons move to distinct final excited or ionized states. In this way, using the IEM, it is possible to distinguish the probabilities of elastic, single-excitation, and double-excitation events. The generalization for more electrons is straightforward.

A general and more compact form of Eq. (1) can be written as

$$\frac{dP_{atom}^{elec}}{d\Delta E}(b) = \left(\prod_i \int dT_i \frac{dP_i}{dT_i}(b) \right) \times \delta\left(\Delta E - \sum_i T_i \right), \quad (2)$$

where the index i runs over all electrons for each subshell (e.g., $2s$, $2p$, $3s$, and $3p$ for a K atom). Here the inner shells ($1s$ for the K atom) have not been taken into account since they are kinematically suppressed for protons at 100 keV. Equation (2) corresponds to a series of convolutions of individual single-electron energy-loss distributions and thus the whole distribution is unitary.

B. Monte Carlo simulations of MEIS energy-loss spectra

In order to calculate the energy-loss spectra relevant to the real MEIS experiment, one must consider the interactions along the scattered ion trajectories using the SILISH code referred to in the Introduction. Briefly, to achieve this, as in the VEGAS program[28] the lattice positions of the adsorbate and substrate atoms are stored in an array. For each impinging projectile, the target atoms are displaced according to their one-dimensional root-mean-square thermal vibrations, and the ion trajectory is determined by a sequence of binary collisions. In each of them, the scattering angle is obtained by using the Moliere scattering potential, the ion energy, and the impact parameter. The scattering angle is used to determine the new ion direction as well as the recoil-energy transfer to the target atom. In contrast to the VEGAS program, however, the impact parameter is also used to select the associated inelastic energy loss tabulated from calculations based on Eq. (2) for different targets and impact parameters. The target atoms are selected by considering the atoms inside a cylinder with radius r_{max} and axis parallel to the ion incident direction.

The flux of incident ions at each lattice position is then stored in a 2D matrix, where each bin, representing the transverse ion position, contains not only the number of projectiles but also the histogram of ion directions and energy losses. The same calculation is performed for the outgoing ions in the detection direction using time reversibility. The incoming and outgoing tracks are connected by using the corresponding flux matrices, together with the position of the backscattering atom according to its thermal vibration. Only trajectories within the same scattering plane are connected. The corresponding energy loss for the whole ion trajectory therefore consists of the energy loss due to the incoming and outgoing paths, as well as to the elastic and inelastic energy loss in the hard scattering collision. In this way, the variation of the kinematical factor due to different scattering angles is also taken into account.

IV. RESULTS AND DISCUSSION

As remarked in the Introduction, the energies and occupation numbers of the shallow core levels of the three alkali metal atoms studied here do vary significantly, with the absence of intermediate-energy d states in K relative to Rb and Cs being particularly significant. We therefore first report the results of the theoretical energy-loss spectra from these three atoms for 100-keV H^+ scattering without the incorporation

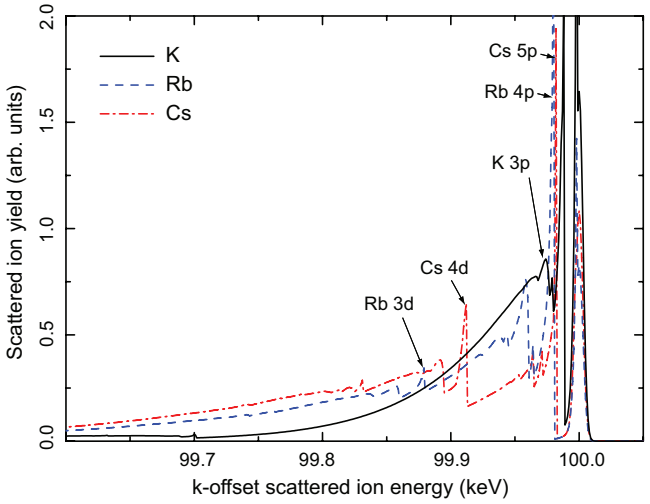

FIG. 1. (Color online) Calculated results for the energy-loss distribution for H^+ ions impinging on isolated atoms of K, Rb, and Cs at small impact parameter. The no-loss features have been convolved with a narrow Gaussian (FWHM approximately 7 eV) in order to broaden them sufficiently to allow their inclusion in the plots and aid visual assessment of their relative importance. The scattered ion energies take no account of elastic-recoil energy loss. Thresholds for single ionization of some of the shallow core levels are labeled.

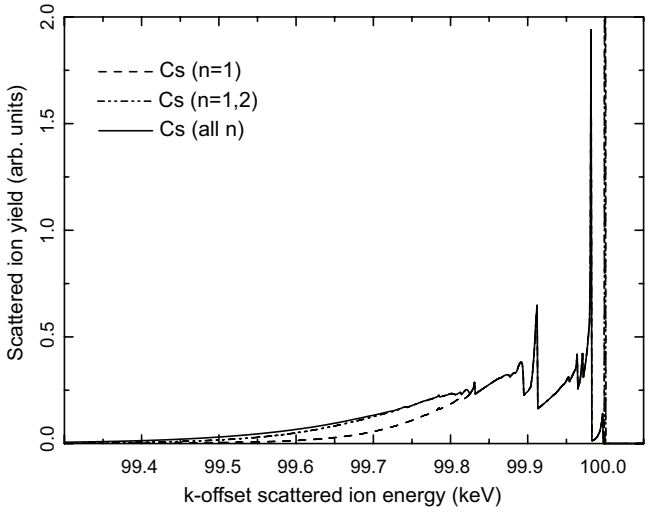

FIG. 2. Calculated results for the energy loss distribution for H^+ ions impinging on isolated atoms of Cs at small impact parameter, showing the contributions of single excitations (and elastic scattering) alone ($n=1$), single and double excitations ($n=1,2$), and all orders of multiple excitation (as shown in Fig. 1). Other details are as in Fig. 1.

of any instrumental broadening. Figure 1 shows the results of the coupled-channel calculations for the energy-loss probability of 100-keV H^+ projectiles colliding with atomic K, Rb, and Cs at an impact parameter, b, close to zero, corresponding to a large scattering angle (note that these spectra are essentially identical for any impact parameter associated with a large scattering angle[8]). In this figure, each elastic peak (located at 100 keV) is convolved with a Gaussian function with a FWHM of 7 eV, in order to allow easier visual comparison of the importance of the no-loss and loss contributions to the whole distribution. Note that the areas of these peaks correspond to the probability of no-loss collisions, namely 12.2% for K, 6.2% for Rb, and 8.1% for Cs. A notable aspect of the energy-loss distribution in Fig. 1 is the significant contribution of excitation of alkali metal subshells at large energy transfers. Some of the main ionization thresholds for the various core electron states are labeled. While there are clearly detailed differences in the energy-loss spectra associated with the different shallow (valence and near-valence) core levels, these effects occur within ~50 eV of the no-loss peak and are unlikely to be resolved in the experiments (with an instrumental resolution of ~250 eV). More notable in this regard is the significantly larger intensity at higher-loss energies in the 200–400 eV range for Rb and Cs, relative to that for K. This difference can be assigned to the role of the d-state excitations and it is these contributions which are expected to give rise to an enhanced asymmetry in the experimental spectra which are subjected to instrumental broadening.

More detailed evaluation of the results of the calculations reveal, however, that multiple excitations play a substantial role in the differences in energy loss between the three alkali atoms in this higher-energy region. In particular Fig. 2 shows the calculated scattered ion energy spectrum for large-angle scattering from isolated Cs atoms if one includes only single excitations and no-loss (elastic) contributions, if one then adds double excitations, and if one includes all orders of excitations (as in Fig. 1). Evidently, for Cs, the contribution of multiple excitations becomes dominant for energy losses greater than approximately 250 eV. Figure 3 shows how the role of these multiple excitations differs for the three alkali atoms. For K there is essentially no contribution from multiple excitations, but for Rb double excitations are significant and for Cs more than 20% of the excitations are double or higher order. These multiple excitations are exclusively for the shallow core levels (L shell for K, M shell for Rb, N shell for Cs) and almost exclusively involve the d states. The major differences in the higher energy losses for the three alkalis are thus attributable to excitations of the d electrons, and particularly multiple excitations of these states.

Evidently, in experimental spectra that suffer significant instrumental broadening, it is the increasing importance of relatively high energy (>100–150 eV) losses for the heavier

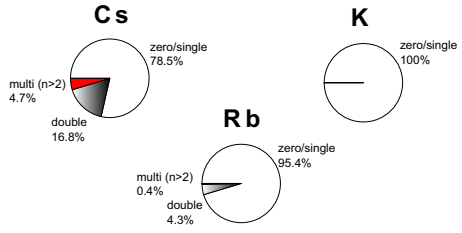

FIG. 3. (Color online) Pie-chart representation of the relative contributions of different orders of excitations to the scattered ion energy spectra for 100-keV H^+ scattering at large scattering angle from K, Rb, and Cs atoms. Zero excitation corresponds to pure elastic scattering, single to single electronic excitations of an atom, etc.

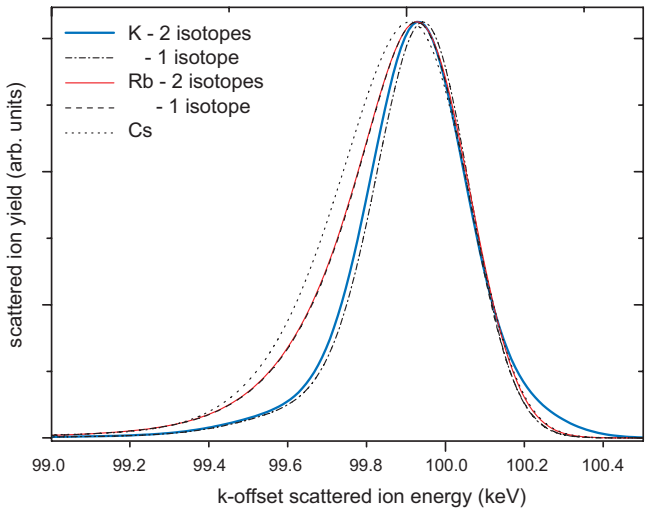

FIG. 4. (Color online) Calculated results for the energy-loss distribution for H^+ ions impinging on isolated atoms of K, Rb, and Cs on Al(111) for 90° scattering calculated using the SILISH code and broadened by convolution with a Gaussian of FWHM 250 eV to represent the instrumental broadening. For Rb and K, the effect of including the two different isotopes is also shown. The scattered ion energy scale has been offset by the kinematic correction associated with the recoil energy loss.

alkali atoms that is expected to be the main observable effect. This expectation is confirmed by the results of Fig. 4, which show theoretical spectra for 90° scattering after broadening by convolution with a Gaussian with a FWHM of 250 eV, the value found to give the best description of the instrumental resolution of the associated experiments. Notice that for scattering from Rb and K, Fig. 4 also shows the difference in the expected spectra for a single isotope, and for the naturally-occurring abundance ratio of the two main isotopes. The additional broadening introduced by the two different masses is actually much more noticeable for K than for Rb, because while the abundance of the dominant isotope is higher for K, the relative difference in the masses of the two components is larger, and the lower-abundance higher-mass isotope leads to a high-energy "tail" on the calculated scattered ion energy spectrum. Note that while Figs. 1–3 show information relating to the energy-loss spectrum extracted directly from the atomic calculation used to generate the loss spectrum as a function of impact parameter, Fig. 4 and subsequent figures, shown to aid experiment/theory comparisons, are based on the use of the SILISH program used to calculate the energy loss over different scattering trajectories for the actual surface structure.

An important issue in comparing theoretical and experimental ion energy spectra is how one deals with the broadening in the experimental data due to instrumental effects, most notably the energy spread in the incident ion beam and the response function of the toroidal ion energy analyzer. Without detailed knowledge of this instrument function, it is clearly important to constrain its permitted form or one can always get a good fit by adjusting this component. In our earlier investigation of scattering from the Si(111)/Y system,[8] we assumed only that the instrument response function must be symmetric, but could take the rather general form that the intensity as a function of energy, E, should be

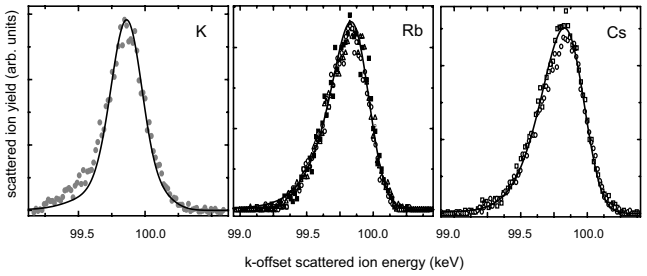

FIG. 5. Comparison of the experimental scattered ion energy spectra from the K, Rb, and Cs overlayers on Al(111) atoms for 90° average scattering angle with the theoretical predictions of Fig. 2. The full lines are the results of the theoretical simulations, and the different symbols correspond to experimental data points from separate measurements. The scattered ion energy scale has been offset by the kinematic correction associated with the recoil energy loss.

$$I = I_0 \exp\{-[\ln(2)/2]|E/FWHM|^w\}.$$

We then also noted that as the expected, unbroadened spectrum (Fig. 1) is highly asymmetric, with a much sharper high-energy cutoff, we should adjust the instrument function to give a good fit to the high-energy side of the experimental peak. Interestingly, this procedure led to a value for the exponent, w, of almost exactly 2; i.e., the optimal instrument function is essentially Gaussian. Based on this, in the present study it was assumed that the instrument function was Gaussian, and only the FWHM value was adjusted to find a value which gave the most consistent fit to the data from all three alkali metals. The resulting value was 250 eV.

Figure 5 shows these same broadened theoretical spectra of Fig. 4 compared with the equivalent experimental spectra, all recorded in the same scattering geometry, with ion incidence along $[\bar{1}\bar{1}0]$ and detection along [001], corresponding to a 90° scattering angle. Clearly the agreement for the Rb and Cs scattering data is excellent, but less good for the K scattering measurements. The origin of the mismatch of theory and experiment in the low-energy side of the K scattering peak is not entirely clear. Our inability to correct for the sawtooth distortion on the two-dimensional detector due to the low scattering signal and poor signal-to-noise ratio, mentioned earlier, may be a contributory factor, although this would be expected to lead to a general broadening and not to the presence of the enhanced intensity in the wings. Increasing the width of the Gaussian function, used in the convolution with the theoretical spectrum to represent the experimental resolution, by 10–20 eV, did lead to a marginal improvement in the overall fit, but failed to address the main discrepancy of the low-energy shoulder in the experimental data. One possible reason for this feature is a small amount of subsurface Ar or K. In initial low-resolution measurements, when Ar ion sputtering was used for sample cleaning, a similar effect was seen but with substantially greater intensity. The data presented here were recorded after a substantial number of cycles of Ne ion sputtering, but it is possible

that a small amount of implanted Ar from the earlier cleaning still remained in the near-subsurface region of the newly prepared surface. The second possibility is the presence of some subsurface penetration of the K. Because of their very large atomic radii, one does not generally expect subsurface penetration of alkali atoms in Al, but K is the smallest of the three atoms investigated, and it is notable that penetration to the second layer of Al(111) is well-established for the even smaller Na atom (e.g., Ref. 29). Deeper penetration has never been reported, but most surface science techniques are relatively "blind" to this effect. In view of the fact that the energy of the low-energy shoulder implies an implanted Ar or K distribution peaking several layers below the surface the interpretation based on Ar seems more probable. Despite this somewhat poorer quantitative fit to the K data, a clear feature of this experimental scattered ion energy peak is that it is significantly narrower and more symmetric than those from Rb and Cs, fully consistent with the theoretical prediction.

One further question we may address is the influence of different scattering geometries on the energy-loss spectrum. In principle, even for an adatom on a surface, the scattering geometry could influence the spectrum through two mechanisms. Firstly, different scattering angles involve different impact parameters in the hard collision, and this difference in the local trajectory of the ions close to the scatterer could influence the energy-loss process, although, as we have remarked above, the atomic calculations indicate very little difference in the energy-loss spectrum for a wide range of scattering angles. Secondly, if the scattering geometry involves either incident or scattered ion trajectories that are grazing relative to the surface, one may expect to see additional broadening due to excitation of electrons associated with the Al substrate atoms. As the experimental scattered ion energy spectrum from Cs shows the strongest asymmetry due to inelastic losses, measurements and calculations have focused on this system as the one most likely to display significant effects. Figure 6 shows the results. In the upper panel are shown experimental spectra recorded in four different scattering geometries: 90° scattering angle (incidence direction $[\bar{1}\bar{1}0]$ and detection along [001], with associated polar incidence and detection angles of 35.26° and 54.74°, respectively, relative to the surface normal); 125.27° scattering angle ($[\bar{1}\bar{1}0]$ incidence, [112] detection, associated polar angles of 35.26° and 19.47°); 100.03° scattering angle ($[\bar{1}\bar{1}\bar{2}]$ incidence, $[33\bar{2}]$ detection, associated polar angles of 19.47° and 60.50°); 125.27° scattering angle ($[\bar{1}\bar{1}\bar{2}]$ incidence, [110] detection, associated polar angles of 19.47° and 35.26°). Notice that the second and fourth geometries (each with a scattering angle of 125.27°) simply involve a switch of ingoing and outgoing trajectories, so the interaction with the Cs atom should be identical. There appears to be no systematic difference between the shapes of these four spectra. In the lower panel are shown a series of theoretical simulations of these experimental geometries (shown in the graph by the same symbols) and of three other geometries not investigated experimentally. The simulations of the experimental data indicate that there should be no discernible difference between the energy-loss spectra in these four different scattering geometries, consistent with our view that the atomic calculations show no differences between these three (large) scattering angles, and that the ion trajectories are too distant from the underlying Al atoms to be influenced by interaction with these substrate atoms. The additional theoretical spectra, however, show that if the ion trajectory is only 10° from grazing, a small additional broadening is seen due to interaction with the Al atoms, and this effect becomes significantly more pronounced for grazing angles of 5° and 3°; notice that for these three geometries the incident ion direction is the same, along $[00\bar{1}]$, but the outgoing trajectory is increasingly grazing.

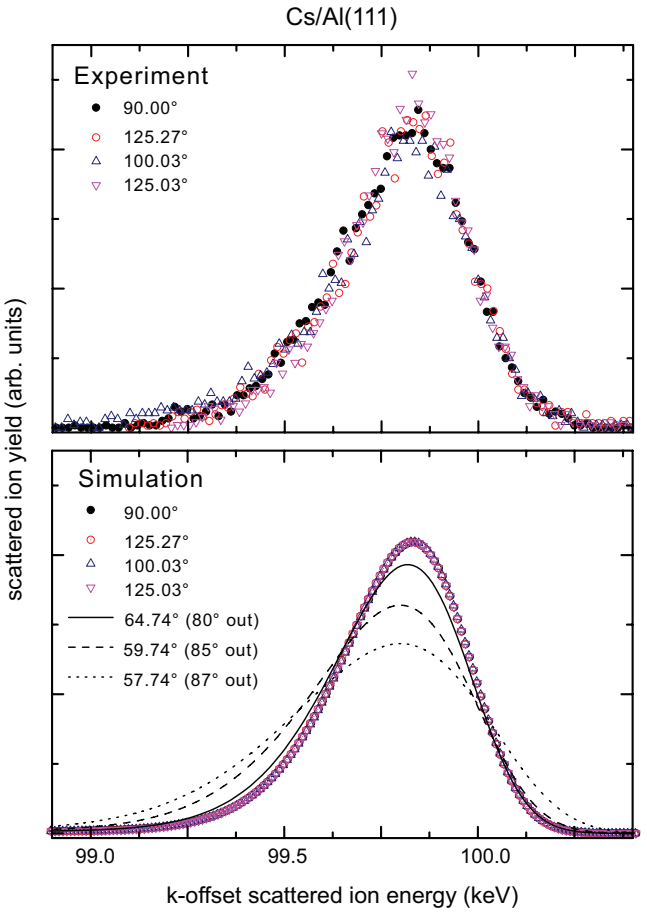

FIG. 6. (Color online) Data showing the influence of different scattering geometries on the energy loss spectrum of 100-keV H^+ ions scattered from Cs adsorbed on Al(111). The upper panel shows experimental data recorded at different scattering angles in scattering geometries described in the text. The lower panel shows the results of simulations for the same scattering geometries and for three other scattering geometries involving more grazing exit angles (polar angles of 80°, 85°, and 87° corresponding to grazing angles of 10°, 5°, and 3°).

V. CONCLUSIONS

The results of our experimental measurements of the scattered ion energy spectra from essentially single-atom scattering of 100-keV H^+ ions from K, Rb, and Cs compare very

favorably with the results of theoretical calculations which consider explicitly the energy loss associated with atomic electronic excitations, a description which promises to allow far more quantitative analysis of MEIS data from ultrathin surface layers. In particular the theoretically predicted pronounced asymmetry of the ion energy spectra scattered from Rb and Cs atoms, which appears to be most strongly related to 3*d* and 4*d* electronic excitations, respectively, and an increasing importance of multiple excitations, is reproduced essentially exactly by the experimental data. For scattering from the K atoms, the experimental spectra reproduce the theoretically predicted near-symmetry of the scattered ion energy peak, but show an additional low-energy shoulder not predicted by the theory; this effect may be attributable to the nature of the sample preparation.

Comparison of the theoretical and experimental results for scattering from Cs adsorbed on Al(111) also show that the energy-loss spectrum is essentially independent of scattering angle for single-atom collisions at large scattering angles, while the results also show that inelastic losses due to interaction with the Al substrate are only significant for very grazing ion trajectories on this surface in which the Cs atoms lies significantly above the near-neighbor Al atoms.

The results appear to be very encouraging for this approach to analysis of the MEIS data aimed at exploiting the best possible (atomic-scale) depth resolution. Further tests involving scattering experiments from well-characterized solid surfaces, in which scattering trajectories involving surface and subsurface inelastic losses, are now being investigated to extend the original investigation of this type on Al(110).

ACKNOWLEDGMENTS

The authors acknowledge funding support by the Engineering and Physical Sciences Research Council (UK), by CNPq and CAPES (Brazil), and by DAAD within the PROBRAL contract (Germany).

*Corresponding author. Electronic address: d.p.woodruff@warwick.ac.uk

[1] J. F. van der Veen, Surf. Sci. Rep. **5**, 199 (1985).
[2] J. F. Ziegler, SRIM code, http://www.SRIM. org
[3] W. K. Chu, Phys. Rev. A **13**, 2057 (1976).
[4] Q. Yang, D. J. O'Connor, and Z. Wang, Nucl. Instrum. Methods Phys. Res. B **61**, 149 (1991).
[5] G. Schiwietz, Phys. Rev. A **42**, 296 (1990); P. L. Grande and G. Schiwietz, Phys. Rev. A **44**, 2984 (1991); G. Schiwietz and P. L. Grande, Nucl. Instrum. Methods Phys. Res. B **69**, 10 (1992); P. L. Grande and G. Schiwietz, Phys. Rev. A **47**, 1119 (1993).
[6] P. L. Grande, A. Hentz, G. Schiwietz, W. H. Schulte, B. W. Busch, D. Starodub, and T. Gustafsson, Phys. Rev. B **69**, 104112 (2004).
[7] A. Hentz, G. S. Parkinson, M. A. Muñoz-Márquez, D. P. Woodruff, P. L. Grande, G. Schiwietz, P. Bailey, and T. C. Q. Noakes (unpublished).
[8] M. A. Muñoz-Márquez, G. S. Parkinson, D. P. Woodruff, A. Hentz, P. L. Grande, G. Schiwietz, T. J. Wood, C. Bonet, S. P. Tear, P. Bailey, and T. C. Q. Noakes, Phys. Rev. B **72**, 075415 (2005).
[9] C. Rogero, C. Polop, L. Magaud, J. L. Sacedón, P. L. de Andrés, and J. A. Martín-Gago, Phys. Rev. B **66**, 235421 (2002).
[10] R. D. Diehl and R. McGrath, Surf. Sci. Rep. **23**, 43 (1996).
[11] C. Stampfl, M. Scheffler, H. Over, J. Burchhardt, M. Nielsen, D. L. Adams, and W. Moritz, Phys. Rev. Lett. **69**, 1532 (1992); C. Stampfl, M. Scheffler, H. Over, J. Burchhardt, M. Nielsen, D. L. Adams, and W. Moritz, Phys. Rev. B **49**, 4959 (1994).
[12] M. Kerkar, D. Fisher, D. P. Woodruff, R. G. Jones, R. D. Diehl, and B. Cowie, Phys. Rev. Lett. **68**, 3204 (1992).
[13] G. Scragg, B. C. C. Cowie, M. Kerkar, D. P. Woodruff, A. Daimellah, S. Turton, and R. G. Jones, J. Phys.: Condens. Matter **6**, 1869 (1994).
[14] M. M. Nielsen, J. Burchhardt, D. L. Adams, E. Lundgren, and J. N. Andersen, Phys. Rev. Lett. **72**, 3370 (1994).
[15] D. L. Adams, Appl. Phys. A **A62**, 123 (1996).
[16] J. N. Andersen, E. Lundgren, R. Nyholm, and M. Qvarford, Surf. Sci. **289**, 307 (1993).
[17] *Photoemission in Solids I: General Principles*, edited by M. Cardona and L. Ley (Springer-Verlag, Berlin, 1978).
[18] P. Bailey, T. C. Q. Noakes, and D. P. Woodruff, Surf. Sci. **426**, 358 (1999).
[19] R. M. Tromp, M. Copel, M. C. Reuter, M. Horn von Hoegen, J. Speidell, and R. Koudijs, Rev. Sci. Instrum. **62**, 2679 (1991).
[20] D. Brown, T. C. Q. Noakes, D. P. Woodruff, P. Bailey, and Y. Le Goaziou, J. Phys.: Condens. Matter **11**, 1889 (1999).
[21] R. M. Tromp, M. Copel, M. C. Reuter, M. Horn von Hoegen, J. Speidell, and R. Koudijs, Rev. Sci. Instrum. **62**, 2679 (1991).
[22] J. Kim, W. N. Lennard, C. P. McNorgan, J. Hendriks, I. V. Mitchell, D. Landheer, and J. Gredley, Curr. Appl. Phys. **3**, 75 (2003).
[23] W. Fritsch and C. D. Lin, Phys. Rep. **202**, 1 (1991); J. F. Reading, T. Bronk, A. L. Ford, L. A. Wehrman, and K. A. Hall, J. Phys. B **30**, L189 (1997).
[24] J. Bang and J. M. Hansteen, K. Dan. Vidensk. Selsk. Mat. Fys. Medd. **31**, 13 (1959); L. Wilets and S. J. Wallace, Phys. Rev. **169**, 84 (1968); M. R. Flannery and K. J. MacCann, Phys. Rev. A **8**, 2915 (1973).
[25] F. Herman and S. Skillmann, in *Atomic Structure Calculations* (Prentice-Hall, Inc., Englewood Cliffs, New Jersey, 1963).
[26] U. Wille and R. Hippler, Phys. Rep. **132**, 129 (1986).
[27] G. Schiwietz, B. Skogvall, J. Tanis, and D. Schneider, Phys. Rev. A **38**, 5552 (1988).
[28] J. W. M. Frenken, R. M. Tromp, and J. F. van der Veen, Nucl. Instrum. Methods Phys. Res. B **17**, 334 (1986).
[29] R. Fasel, P. Aebi, L. Schlapbach, and J. Osterwalder, Phys. Rev. B **52**, R2313 (1995).